MICROMACHINED THIN FILM PLATE ACOUSTIC RESONATORS (FPAR): THEORY AND APPLICATIONS

V. Yantchev and I. Katardjiev

Uppsala University, Dept. Solid State Electronics, Box 534, 75121 Uppsala, Sweden
E-mail: veya@angstrom.uu.se , URL: http://hermes.teknikum.uu.se/~veya

I. INTRODUCTION

Thin film plate acoustic resonators (FPAR) represent novel class of integrated circuit compatible resonators utilizing guided modes in AlN (Aluminium Nitride) thin film membranes. Among the variety of plate guided waves, the lowest order symmetric lamb wave (S0) has attracted specific interest due to its weak dispersion, high velocity >10000) and moderate electromechanical coupling. The mode in question has extensional nature of vibration determining thus a predominantly longitudinal wave polarization. First results on this type of resonators have been published in peer reviewed journal in 2005 [1] although similar approach on quartz has been independently demonstrated earlier [2]. Currently two types of resonators employing the S0 Lamb wave in AlN membranes are being developed. The first one, utilize reflections from the edges of a suspended membrane [3,4] (found in literature as LWR (Lamb wave resonators) or Contour-extensional mode resonators), while the other utilize reflections from periodic strip gratings representing distributed reflectors (Bragg type) similar to the reflectors used in surface acoustic wave (SAW) resonators [5, 6]. Both design types of resonators utilize inter-digital transducers (IDT) for excitation of the S0 Lamb wave. When acoustically thin plates are considered S0 Lamb waves are predominantly being excited through the e31 piezoelectric coefficient independently on the IDT topology (with or without bottom electrode). The latter represents a lateral field excitation i.e the S0 Lamb wave is being excited mostly by the components of the external electric field normal to the wave propagation direction. The use of the same transducer topology as in SAW micro-devices enables an almost straightforward application of the SAW modelling techniques to the specific case of Lamb waves. Further the S0 Lamb wave being the lowest order in the plate can not convert during reflections to other Lamb modes as far as their cut-off frequencies lay above the frequency of the S0 Lamb wave (i.e S0 mode in acoustically thin plates). The latter along with the weak velocity dispersion in acoustically thin plates determine a mode with SAW-like properties (i.e strongly guided, with no conversion losses and weak dispersion).

II. ANALYSIS

As discussed above applying SAW design methods appears to be physically sound provided that some work regarding their adaptation to the specific nature of the S0 Lamb wave is done. So far FEM/BEM and Green function analysis have been demonstrated successfully in plate wave analysis [7,8]. According to the authors experience COMSOL and Ansys FEM-based software can also be successfully used. Here we briefly discuss the applicability of the more robust Couplings-of-Modes Analysis (COM) [9] giving straight access to the device physics, which could remain hidden in the more complicated FEM-based analysis. Most generally COM is a phenomenological model for guided wave propagation and excitation, which is widely employed for the design of high-performance, SAW devices [10]. The analysis based on the COM model gives very simple and analytical solutions with a surprisingly good accuracy provided that the COM parameters are properly determined. COM model has been used with some success to describe dispersive SAWs in layered structures as well as leaky surface acoustic waves exhibiting bulk losses and premature stopband degradation. In comparison to the latter the S0 Lamb wave demonstrates weak dispersion and well defined waveguiding. Conversion losses induced by reflection are known to be suppressed in acoustically thin plates presuming thus relative simplicity of the loss mechanisms. The COM equations used in this study are [10]:

$$\begin{aligned}
\frac{dR(x)}{dx} &= -j\delta R(x) + jk_{12}S(x) + j\alpha V \\
\frac{dS(x)}{dx} &= -jk_{12}R(x) + j\delta S(x) - j\alpha V \quad , \qquad (1) \\
\frac{dI(x)}{dx} &= -2j\alpha R(x) - 2j\alpha S(x) + j\omega CV
\end{aligned}$$

where *R(x)* and *S(x)* are slowly varying fields describing the amplitudes of the forward and the backward propagating modes, k_{12} is the COM reflectivity parameter, α is the COM transduction coefficient, C is the transducer capacitance per unit length, V is the applied voltage and $\delta = (\omega / v[\omega]) - (\pi / p) - j\gamma$ is a detuning parameter describing the effects of the unperturbed velocity dispersion and the propagation losses induced by the material viscosity and the wave diffraction. Here ω is the angular frequency, $v[\omega]$ is the dispersive unperturbed velocity, $p=\lambda_0/2$ is the grating pitch and γ is the acoustic attenuation. For convenience here we present the COM parameters described above in normalized fashion:

- $k_P = -k_{21} \cdot \lambda_0$ —dimensionless reflectivity per finger pair, where k_{21} is the COM reflectivity parameter and λ_0 is the IDT period;
- v_{S0} – S0 Lamb wave unperturbed velocity in AlN at central frequency $f_0 = v_{S0} / \lambda_0$;
- αn —normalized COM transduction coefficient, $\alpha n = \frac{\alpha \cdot \lambda_0}{\sqrt{W / \lambda_0}}$, where *W* is the device aperture, and α is the COM transduction coefficient;
- $\gamma_P = \gamma \cdot \lambda_0$ – attenuation per wavelength [Np/λ];
- D — dimensionless velocity dispersion ($v[\omega] \approx v_{S0}(1 - D\frac{\omega - \omega_0}{\omega_0})$), which is empirically extracted from $(\omega - \omega_0)/\omega_0 = (1 - D) \cdot (k - k_0)/k_0$, where $D = 1 - v_{GR}/v_{S0}$, $v_{GR} = \partial\omega / \partial k$ is the Lamb wave group velocity and $k_0 = 2\pi / \lambda_0$ is the wavenumber at central frequency *ω0*;
- Cn —Normalized Capacitance [F/m] (per IDT pair, per unit aperture).

COM parameters related to propagation effects can readily be estimated by means of Floquet-Bloch analysis of the S0 Lamb wave propagation characteristics in periodic strip grating configurations. In this analysis strip boundary conditions to a first order of approximation for the resulting stresses are first applied [11]. The Lamb wave dispersion in plates with thickness d significantly smaller than the acoustic wavelength is determined by the presence of a frequency stopband (see Fig. 1a) with an upper stopband edge relatively insensitive to electrode thickness (h) variations. The observed effect has a relatively complex nature due to a variety of factors acting simultaneously [11]. Further studies on the impact of the non-linear boundary stresses terms on the stopband edge behaviour have identified the possibility to achieve compensated (zero) sensitivity of the upper stopband edge with respect to the electrode thickness (See Fig. 1b) [9]. This finding appears to be technically important, since FPAR resonators naturally operate in the vicinity of the upper stopband edge.

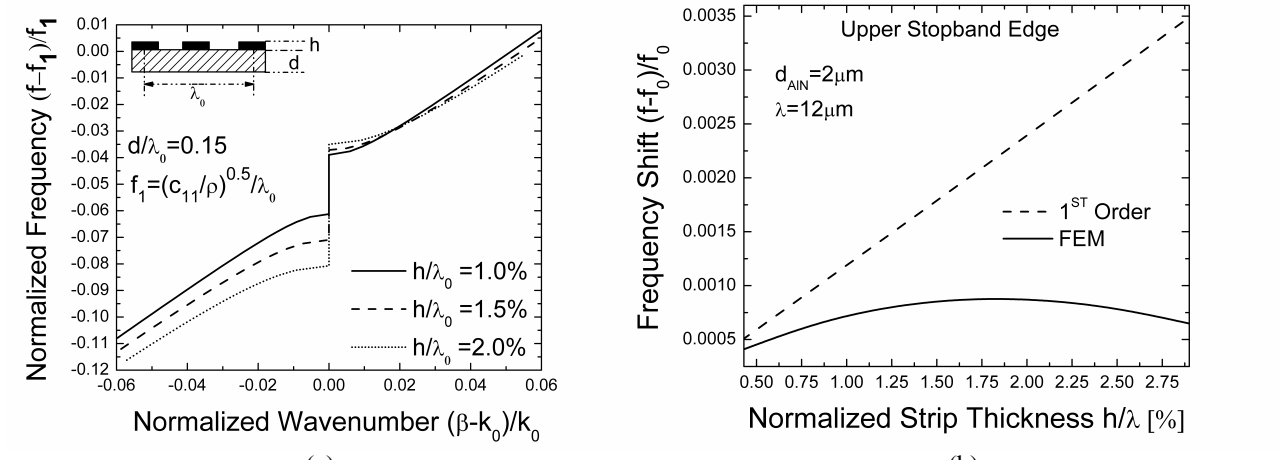

(a) (b)

Figure 1. Propagation Characteristics of the S0 Lamb wave in infinite gratings a) Stopband b) 0-sensitivity of the upper stopband edge.

COM parameters related to S0 Lamb wave excitation and transducer capacitance can be readily derived by means of the effective permittivity approach in quasi-static approximation [9, 12]. In Fig. 2a, the normalized capacitances calculated for two major types of IDT transducers are shown respectively. The first type is a regular IDT, while the second type is an IDT over a floating bottom electrode. In Fig. 2b, the normalized COM transduction coefficients calculated for the two major types of transducers are shown. The agreement between the COM-extracted and theoretically predicted values is found excellent [9].

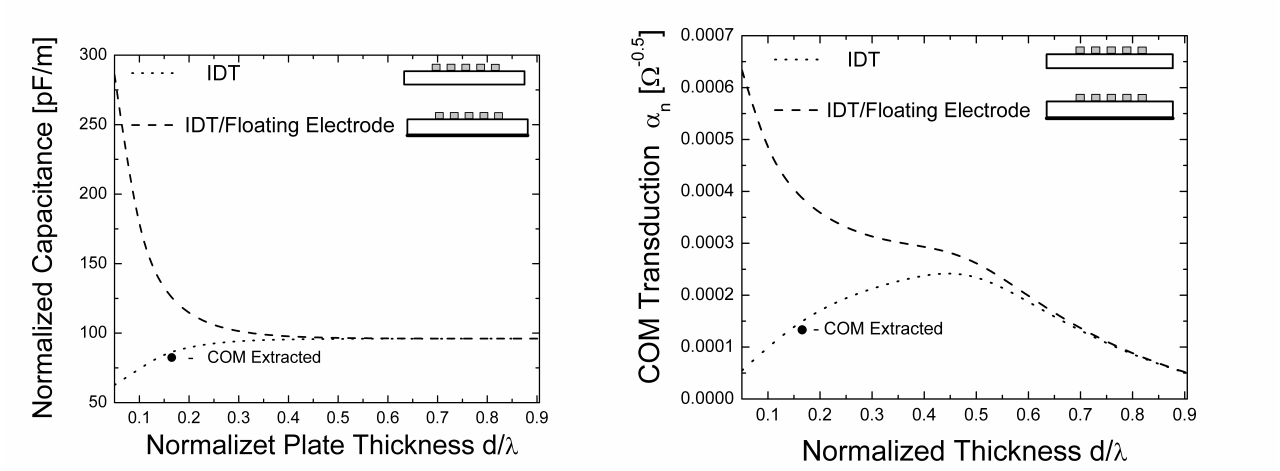

(a) (b)

Figure 2. Transducer Parameters a) Normalized Capacitance b) Normalized COM transduction

Evidently, the IDT/Floating electrode transducer offers a much higher transduction coefficient at relatively small plate thickness to wavelength ratios. More precise evaluation of both the capacitance and the transduction coefficient can be achieved by extracting the COM parameters from the harmonic admittance computed by the FEM/BEM approach adapted to this specific case.

III. FPARs: THEORY VS EXPERIMENTS

The micromachining technology of FPAR is very close to the technology of the thin film bulk acoustic wave resonators (FBAR). Here we show single- and two- port resonators with relatively simplified topology requiring only thin AlN film and patterned top electrode structure. The topology is similar to that of the classical SAW resonators. More experimental results are reported in [5, 6].

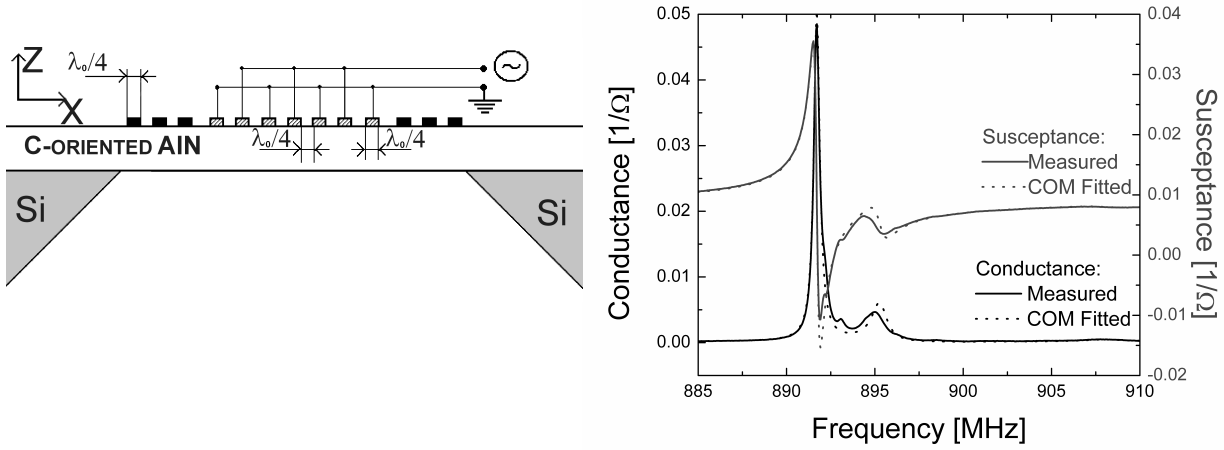

(a) (b)

Figure 3. Synchronous one-port FPAR a) sketch view b) Close in resonance response

In Fig. 3a sketch view of a classical 1-port FPAR is shown. FPARs with synchronous design have been fabricated demonstrating Q factors in air close to 2000 at about 890MHZ resonance frequency (see Fig. 3b). Further, is verified. Further, the excellent match between COM-fitted and measured FPAR response verifies the applicability of the COM approach to the FPAR design. Further improvement in FPAR resonance Q in air was obtained by designing the resonator to operate in the vicinity of the stopband centre [6] gaining thus maximum reflectivity from the reflectors gratings at the expense of slight reduction in the transduction efficiency (see Fig. 4).

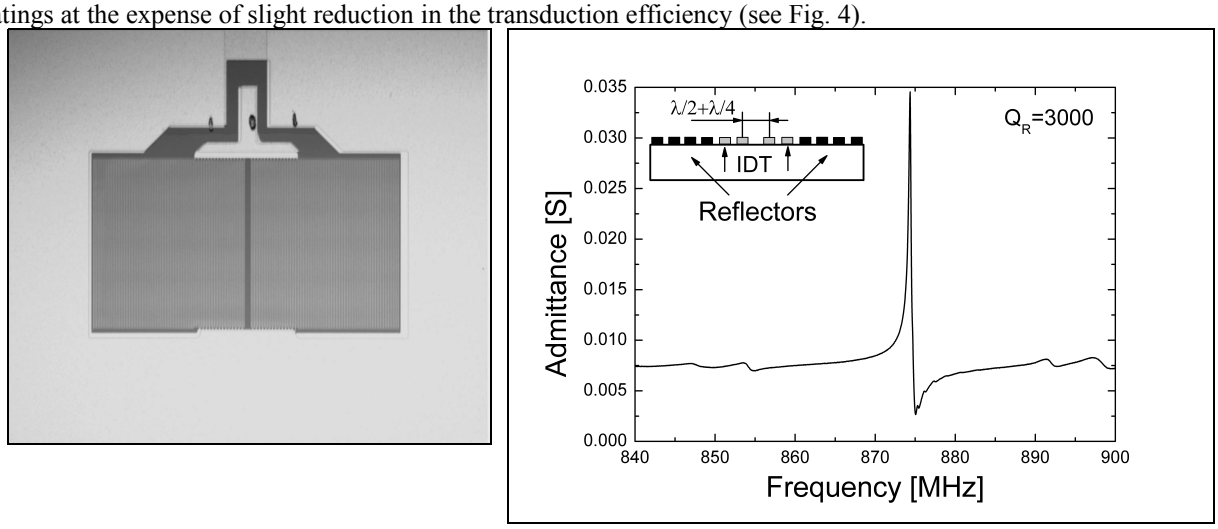

(a) (b)

Figure 4 Hiccup FPAR a) as fabricated b) close in resonance response

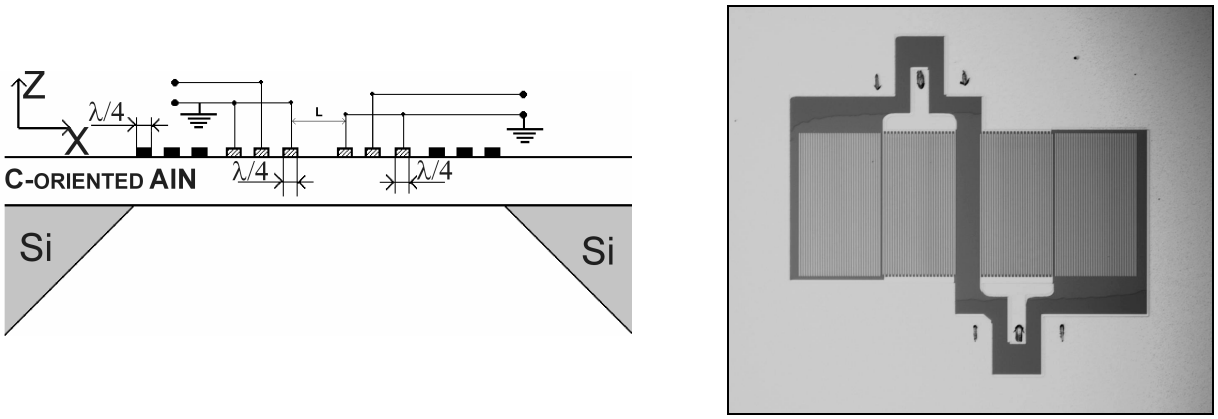

(a) (b)

Figure 5 2-port FPAR a) sketch view b) as fabricated

In Fig. 5 basic topology of the 2-port FPAR is shown. 2-port FPARs have been designed and micromachined, demonstrating unloaded Q in air of 3150 and insertion losses of -3.87dB (see Fig. 6a). Excellent agreement between the experiment and the COM-analysis is further demonstrated (see Fig. 6b).

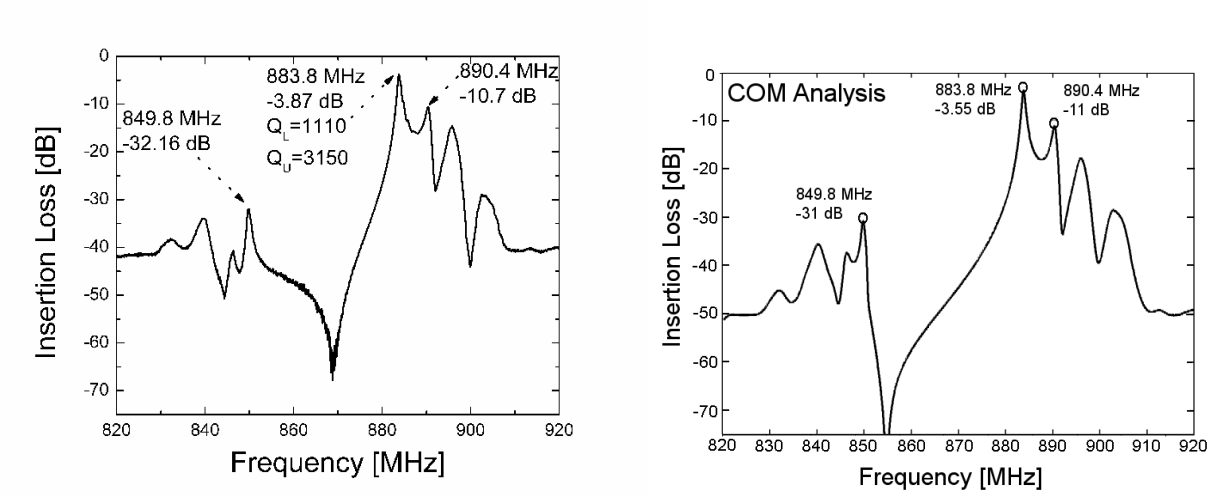

Figure 6 Close in resonance response of a 2-port FPAR a) measured transmission b) COM predicted transmission

IV. TEMPERATURE COMPENSATION

In the proposed work composite membranes consisting of reactively sputtered AlN and the thermally grown SiO2 are used as a platform for the design of temperature-compensated FPAR since the two materials exhibit opposite temperature coefficients of frequency (TCF). The propagation characteristics of the S0 mode in an AlN/SiO2 composite plate are determined by using Adler's algorithm [13], taking into account the temperature dependence of the material constants. The influence of the periodic gratings over the thermal response is neglected in this approximate analysis. Accordingly, the results discussed below should be accepted as ideal and may slightly differ from experiment due to inhomogeneous electrical excitation and mass loading.

In Fig. 7, the temperature coefficient of frequency defined as the relative frequency change per 1 K of temperature variation is shown as a function of the relative SiO2 layer thickness for different relative thicknesses of AlN. It is noted that thicknesses are normalized with respect to the acoustic wavelength (λ) at room temperature as defined from the grating pitch (see figure 2): λ=2Λ, where Λ is the grating pitch. The relative AlN thickness of interest lies in the range where the S0 mode exhibits low dispersion (acoustically thin plate), and in addition where the TCF exhibits a relatively weak dependence on the thickness (see Fig. 7). In this specific range of AlN acoustic thicknesses, temperature compensation can be achieved with SiO2 of thicknesses smaller than that of AlN. The wide applicability of the results obtained with respect to the frequency of operation required is also noted. For a desired frequency of operation the optimal AlN/SiO2 combination is to be chosen among the range of solutions shown in Fig. 7. From those solutions, the one that offers a reasonable trade-off between electromechanical coupling and robustness of fabrication is to be chosen.

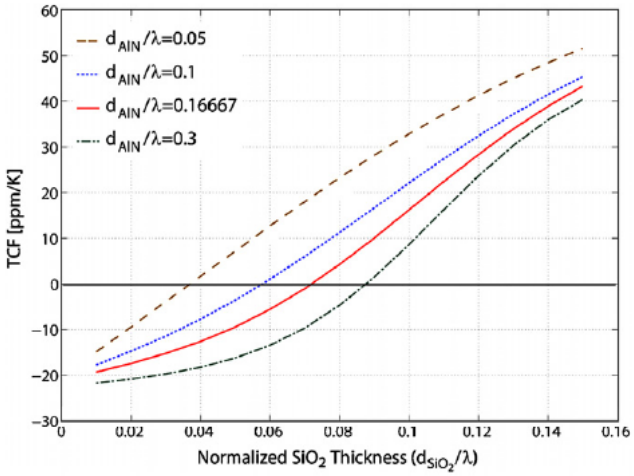

Figure 7. Temperature coefficient of frequency as a function of the SiO2 thickness for AlN plates of varying thicknesses normalized to the wavelength (λ).

Specific design roles for thermally compensated FPAR have been recently discussed [14]. A micromachined thermally compensated 1-port FPARs have been successfully demonstrated exhibiting second order temperature coefficient of frequency $\beta = -31 ppb/K^2$, and Q in air of 1360 at resonance frequency of 755MHz (see Fig 8a,b) [14].

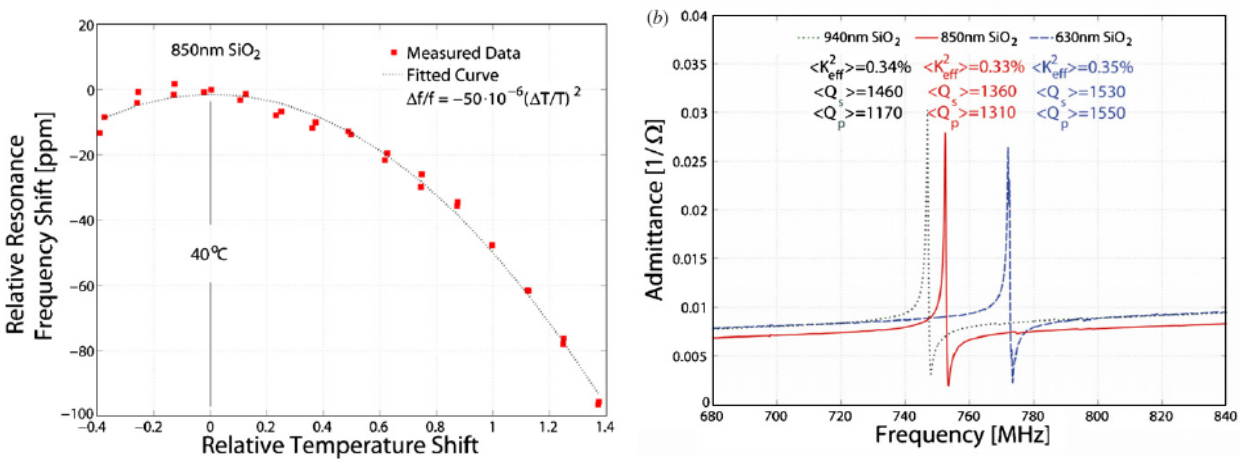

Figure 8. Temperature Compensated FPAR a) measured Relative resonance frequency shift around 40 ◦C for a temperature-compensated synchronous FPAR b) admittance magnitude response for varying SiO2 thicknesses

It is further noted that resonators with second order temperature coefficient of frequency as low as -22.3 ppb/K^2 have been recently demonstrated, when using acoustically thinner composite membrane [15].

V. LOW NOISE FPAR OSCILLATORS

The 2-port FPARs have been micromachined on a free standing AlN membrane. 6mm x 6mm FPAR chips with large contacting pads have been fabricated on to a (100) oriented high resistive 4-inch Si wafer (Fig. 9).

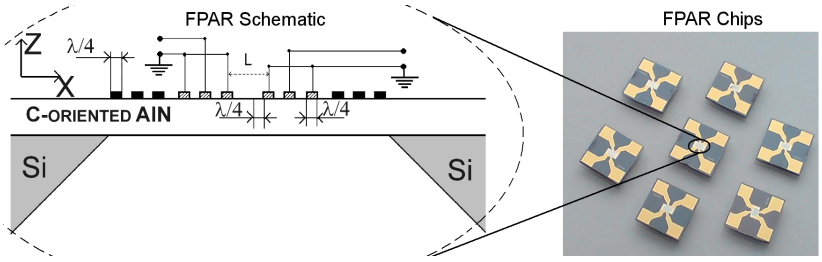

Figure 9. 2-port FPAR devices used in the oscillator

The narrowband transmission (S21) and group delay responses of one of the FPARs used in this study are shown in Fig. 10a. The electrical behaviour is very similar to a synchronous two-port surface acoustic wave (SAW) resonator. To test the power handling ability of the FPAR, the device from Fig. 9 was connected to a power oscillator loop as shown in Fig. 10b. A broadband modular UTO-1023 power amplifier, capable of generating 0,5W of RF power at 1 GHz was used as the power sustaining amplifier in the loop. Except for its high power, this amplifier is also known for its extremely low residual 1/*f* noise, measured as -140 dBc/Hz at 1 Hz carrier offset in this frequency range. In this experiment, the FPAR was run at 24 dBm (250 mW) at f_0 for 5 days. No measurable performance degradation or departure from the data in Fig. 10a was observed after the power handling test, indicating that the FPAR is probably capable of sustaining even greater power levels. Accordingly, the peak stress levels $|T_{11}|_P$ in the FPARs operating at 250mW drive power are found to be in the range of $3 \cdot 10^8 N/m^2 \div 4 \cdot 10^8 N/m^2$ [16]. It is noted that SAW resonators with pure aluminium metallization show irreversible degradation due to acoustically induced migration at stress peak levels exceeding $|T_{11}|_P = 6 \cdot 10^7 N/m^2$. Evidently, the FPAR can sustain at least 6 times larger peak stresses than their SAW counterparts on quartz.

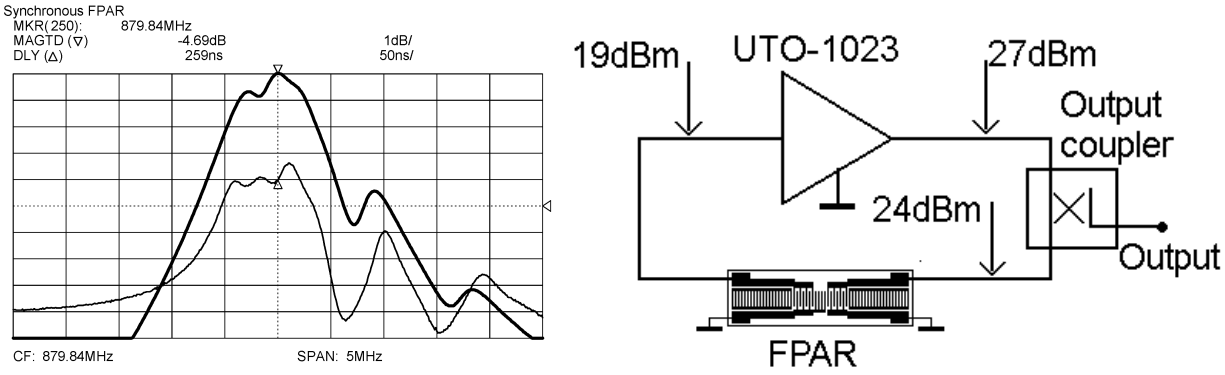

(a) (b)

Figure 10 Oscillator Test a) Transmission close in resonance FPAR characteristics b) Schematics of the loop

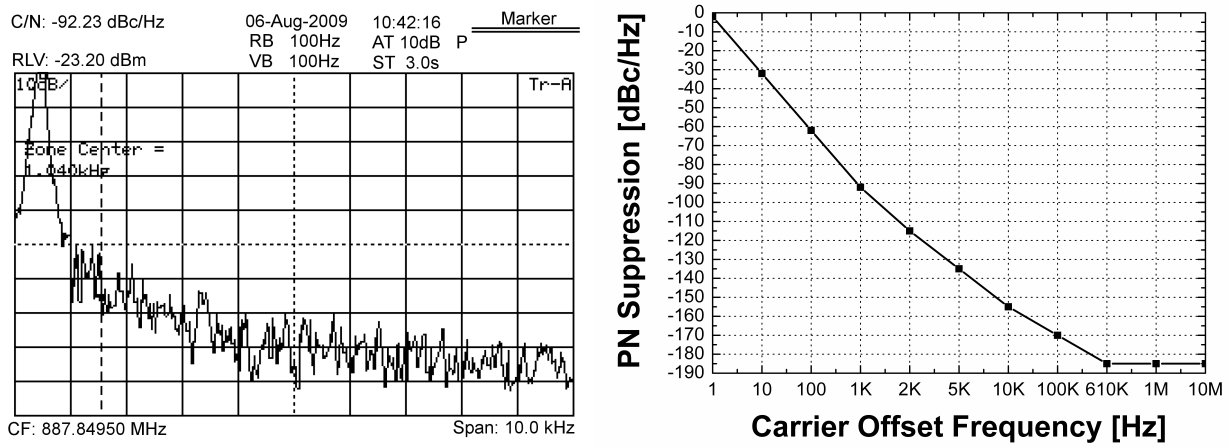

(a) (b)

Figure 11 Oscillator Data a) single-side-band noise spectrum b) phase noise suppression

Despite the relatively low loaded QL=720 the oscillator in Fig. 10b was found to provide a remarkable phase noise performance, as evident by the single-side-band noise spectrum in Fig. 11a measured in the signal-to-noise (S/N) ratio mode of the SA. This measurement allows reading a few data points directly from the noise plot and then making a rough estimate of the overall phase noise performance by taking into account that the close to carrier phase noise follows a 30 dB/decade slope (see Fig, 11b). The thermal noise floor TNF is further calculated as -185dBc/Hz [16]. With a power handling capability exceeding 0.25W and a flicker noise constant of 2.1×10^{-36}/Hz this technology may be very competitive for the manufacture of integrated microwave power oscillators in the near future [16].
It is further noted that oscillator using the physically similar contour extensional mode has demonstrated phase noise of –81 dBc/Hz at 1 kHz offset supporting the applicability of S0 Lamb wave resonators in low noise oscillators [17].

VII. CONCLUSION

This work presents some of the most important results regarding the development of thin film plate acoustic wave resonators at Uppsala University, Sweden. Current studies are focused on the estimation of the sensing capabilities of the S0 FPAR with respect to mass and pressure. The potential of this technology is yet to be realized. Other modes like the first asymmetric and the first symmetric Lamb waves can be of interest too. The first one can be promising candidate for chemical sensor utilizing visco-elastic organic films due to its quasi shear nature [6, 18], while the second one could be promising for building resonators with significantly higher electromechanical couplings [6, 18].

ACKNOWLEDGEMENTS

This work has been funded by the Swedish Research Council (VR).

REFERENCES

[1] J. Bjurström, I. Katardjiev, V. Yantchev, "Lateral-fieldexcited thin-film Lamb wave resonator," Appl. *Phys. Lett*., vol. 86, art. no. 154103, 2005.

[2] Y. Nakagawa et. al., "Lamb wave type high frequency resonator", *Jpn. J. Appl. Phys*., vol. 42, pp. 3086-3090, 2003.

[3] A. Volatier, G. Caruyer, D. Pellissier Tanon, P. Ancey, E. Defaÿ, "UHF/VHF resonators using Lamb waves co-integrated with Bulk Acoustic Wave resonators", *Proc. 2005 IEEE Ultrasonics Symposium*, pp. 902 -905, 2005

[4] P. J. Stephanou and A P. Pisano, "GHZ Contour Extensional Mode Aluminum Nitride MEMS Resonators", *Proc. IEEE Ultrason. Symp.*, pp. 2401-2404, 2006

[5] V. Yantchev and I. Katardjiev, "Micromachined Thin Film Plate Acoustic Resonators Utilizing the Lowest Order Symmetric Lamb Wave Mode", *IEEE Trans. Ultrason., Ferroelect., Freq. Contr*., vol. 54, no. 1, pp. 87-95, 2007

[6] V. Yantchev, L. Arapan, I. Katardjiev, " Micromachined Thin Film Plate Acoustic Wave Resonators (FPAR): Part II", *IEEE Trans. Ultrason., Ferroelect*., *Freq. Contr*., vol. 56, No. 12, pp. 2701 – 2710, Dec. 2009

[7] T. Pastureaud, W. Daniau, V. Laude, M. Wilm, Y. Malecamp, and S. Ballandras, "Characterization and prediction of transverse plate resonators built using mixed strip and groove gratings," in *Proc. 2001 IEEE Ultrason. Symp*. , pp. 93–96, 2001

[8] Jan Kuypers and Albert Pisano, "Green's Function Analysis of Lamb Wave Resonators", *Proc. 2008 IEEE Int. Ultrason. Symp.*, pp. 1548-1551, 2008

[9] V. Yantchev, "Coupling-of-Modes Analysis of Thin Film Plate Acoustic Wave Resonators utilizing the S0 Lamb mode", *IEEE Trans. Ultrason., Ferroelect., Freq. Contr*., vol. 57 , No. 4 , pp. 801 -807, April 2010.

[10] V. Plessky and J. Koskela, in *Advances in Surface Acoustic Wave Technology, Systems and Applications*. vol. 2, pp. 1– 82, Singapore: World Scientific Publ., 2001.

[11] V. Yantchev and I. Katardjiev, "Propagation characteristics of the fundamental symmetric Lamb wave in thin aluminum nitride membranes with infinite gratings," *J. Appl. Phys*., vol. 98, pp. 849101–849107, Oct. 2005

[12] V. Yantchev and I. Katardjiev, "Quasi-static transduction of the fundamental symmetric Lamb mode in longitudinal wave transducers," *Appl. Phys. Lett*., vol. 88, pp. 214101–214103, 2006.

[13] E. Adler, "Matrix methods applied to acoustic waves in multilayers", IEEE Trans. UFFC, vol. 37, No. 6, pp. 485–490, 1990.

[14] G. Wingqvist, L. Arapan, V. Yantchev and I. Katardjiev, "A micromachined thermally compensated thin film Lamb wave resonator for frequency control and sensing applications," *J. Micromech. Microeng*., Vol. 19, art. no. 035018, 2009

[15] C. M. Lin, T. T. Yen, Y. J. Lai, V. Felmetsger, M. Hopcroft, J. Kuypers, A. Pisano, "Experimental Study of Temperature-Compensated Aluminum Nitride Lamb Wave Resonators", *Proc. 2009 IEEE Int. Freq. Contr. Symp*., pp. 5 -9, 2009

[16] I. Avramov, L. Arapan, I. Katardjiev, V. Strashilov, V. Yantchev, "IC-compatible Power Oscillators Using Thin Film Plate Acoustic Resonators (FPAR)", *Proc. 2009 IEEE Int. Ultrason. Symp*., In Print

[17] C. Zuo, J. Van der Spiegel, G. Piazza, "1.05 GHz CMOS Oscillator based on Lateral-Field-Excited Piezoelectric AlN Contour-Mode MEMS Resonators", Proc. *2009 IEEE Int. Freq. Contr. Symp*., pp. 70 -74, 2009

[18] E. Milyutin, S. Gentil, P. Muralt, "Shear mode bulk acoustic wave resonator based on c-axis oriented AlN thin film", *J. Appl. Phys*., vol. 104, pp. 084508 1 - 6, 2008.